

A review of MBE grown 0D, 1D and 2D quantum structures in a nanowire

Cite this: *J. Mater. Chem. C*, 2013, **1**, 4300

Maria de la Mata,^a Xiang Zhou,^b Florian Furtmayr,^c Jörg Teubert,^c Silviya Gradečak,^b Martin Eickhoff,^c Anna Fontcuberta i Morral^d and Jordi Arbiol^{*ae}

We review different strategies to achieve a three-dimensional energy bandgap modulation in a nanowire (NW) by the introduction of self-assembled 0D, 1D and 2D quantum structures, quantum dots (QDs), quantum wires (QWRs) and quantum wells (QWs). Starting with the well-known axial, radial (coaxial/prismatic) or polytypic quantum wells in GaN/AlN, GaAs/AlAs or wurtzite/zinc-blende systems, respectively, we move to more sophisticated structures by lowering their dimensionality. New recent approaches developed for the self-assembly of GaN quantum wires and InAs or AlGaAs quantum dots on single nanowire templates are reported and discussed. Aberration corrected scanning transmission electron microscopy is presented as a powerful tool to determine the structure and morphology at the atomic scale allowing for the creation of 3D atomic models that can help us to understand the enhanced optical properties of these advanced quantum structures.

Received 25th March 2013
Accepted 9th May 2013

DOI: 10.1039/c3tc30556b

www.rsc.org/MaterialsC

^aInstitut de Ciència de Materials de Barcelona, ICMA-B-CSIC, Campus de la UAB, E-08193 Bellaterra, CAT, Spain. E-mail: arbiol@icrea.cat; Web: www.icmab.cat/gaen

^bMassachusetts Institute of Technology, Cambridge, MA 02139, USA

^cPhysikalisches Institut, Justus-Liebig-Universität Gießen, Heinrich-Buff-Ring 16, DE-35392 Gießen, Germany

^dLaboratoire des Matériaux Semiconducteurs, Ecole Polytechnique Fédérale de Lausanne, 1015 Lausanne, Switzerland

^eInstitució Catalana de Recerca i Estudis Avançats (ICREA), E-08010 Barcelona, CAT, Spain

1 Introduction

Semiconductor nanowires (NWs) are used as building blocks for a new generation of advanced devices intended for different applications: functional nanoelectronics,^{1,2} advanced optoelectronics (light emitting diodes (LEDs) and lasers),^{3–5} single molecule sensing,^{6,7} optochemical sensors,^{8,9} high mobility field effect transistors,¹⁰ batteries,^{11,12} solar cells^{13–16} and thermoelectric devices.^{17,18} In parallel, the use of nanowire heterostructures has



María de la Mata graduated in Chemistry at Universidad de Oviedo (Spain) in 2009. She obtained her MSc in Materials Science at Universitat Autònoma de Barcelona (UAB), under the supervision of Prof. J. Arbiol. She is currently a PhD student in the Group of Advanced Electron Nanoscopy (GAeN) at Institut de Ciència de Materials de Barcelona, ICMA-B-CSIC. Areas of her research interests include:

advanced electron micro/nanoscopy applied to nanomaterials and direct correlation between structure and chemical composition at the nano and atomic scale with the physical properties. She is especially interested in atomic resolution imaging, including light atoms, and polarity induced growth mechanisms in non-planar semiconductor nanostructures.

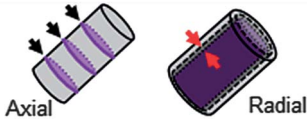
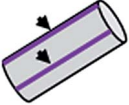
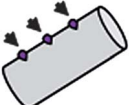


Silviya Gradečak obtained her PhD in Physics from the Swiss Federal Institute of Technology in Lausanne, Switzerland. After receiving Swiss National Science Foundation Fellowship for Prospective Researchers, she was appointed as a Postdoctoral Research Fellow at Harvard University. She joined the MIT faculty in September 2006, where she is currently the Thomas Lord Associate

Professor of Materials Science and Engineering. Her interdisciplinary research program is based on synthesis of nanostructured materials and their assembly into functional devices for applications in nanophotonics, nanoelectronics, and in energy harvesting and conversion. Silviya received several awards, including NSF CAREER Award, inaugural Nano Letters Young Investigator Lectureship, and 3M Innovation Award.

provided an excellent environment for the study of quantum mechanics related phenomena that could lead to applications in emerging fields such as quantum information and technology.^{19–22} Compared to planar structures, semiconductor nanowires show stronger coupling with light, turning the structures into better emitters (when used as LEDs) or absorbers (for solar cells).^{23–25} Moreover, in order to achieve different heterostructures they offer the possibility of two growth directions, *i.e.*, axial and radial. In the case of the axial growth, even the combination of highly mismatched materials is allowed thanks to the radial strain release when the NWs are thin enough.²⁶ In that context, mastering the control of the nanowire morphology, structure and composition has been shown to be a key factor.²⁷ Furthermore, the formation of heterostructures within the

Table 1 Sketch summary of the different quantum structure types attending to the number of confined dimensions

Confined dimensions	Quantum structures	Sketch
1D	Quantum wells, QWs (2D)	 Axial Radial
2D	Quantum wires, QWRs (1D)	
3D	Quantum dots, QDs (0D)	



Martin Eickhoff graduated in Physics from the University of Dortmund in 1995. He worked on SiC materials and microsensor development with DaimlerBenz Research and Technology and received his PhD in Experimental Physics from the Technische Universität (TU) München in 2000. After working for Infineon Technologies AG, Munich he joined the Walter Schottky Institute, TU München from 2001 to 2008 as a

work group leader of the “Sensors and Materials” group. Since 2008 he has been Professor of Experimental Physics at the Justus-Liebig-Universität Giessen. In his work he focuses on the growth and characterization of wide band gap semiconductors (AlGaIn, ZnMgO) as well as their hetero- and advanced nanostructures for application in (bio)chemical sensors and optoelectronics.



Anna Fontcuberta i Morral graduated in physics from Universitat de Barcelona (UB) in 1997. In 2001 she finished her PhD in Ecole Polytechnique in France on polymorphous silicon for thin film photovoltaics. Then, she worked as a postdoc in the group of Harry A. Atwater at Caltech, with whom she co-founded in 2004 the startup company Aonex Technologies. In 2005 she became team leader at

Technische Universität München, where she started research on III–V nanowires. Since 2008 she has been an assistant professor at EPFL, where she has established research on catalyst-free growth of III–V nanowires, related heterostructures and application to photovoltaics.



Jordi Arbiol graduated in Physics from Universitat de Barcelona (UB) in 1997. He obtained his PhD (PhD Extraordinary Award) in 2001 at UB. He was an assistant professor at UB. In 2009 he became ICREA Research Professor at Institut de Ciència de Materials de Barcelona, ICMAB-CSIC. He is currently the leader of the Group of Advanced Electron Nanoscopy and Scientific Supervisor of the

electron microscopy facilities at ICMAB-CSIC. He is a member of the Executive Board of the Spanish Microscopy Society (SME). He has been project Advisor for ANEP, CSIC, ASF, ANPCyT and is currently USP member for the FP7 EU Program I3 ESTEEM2 and for the INA-LMA.

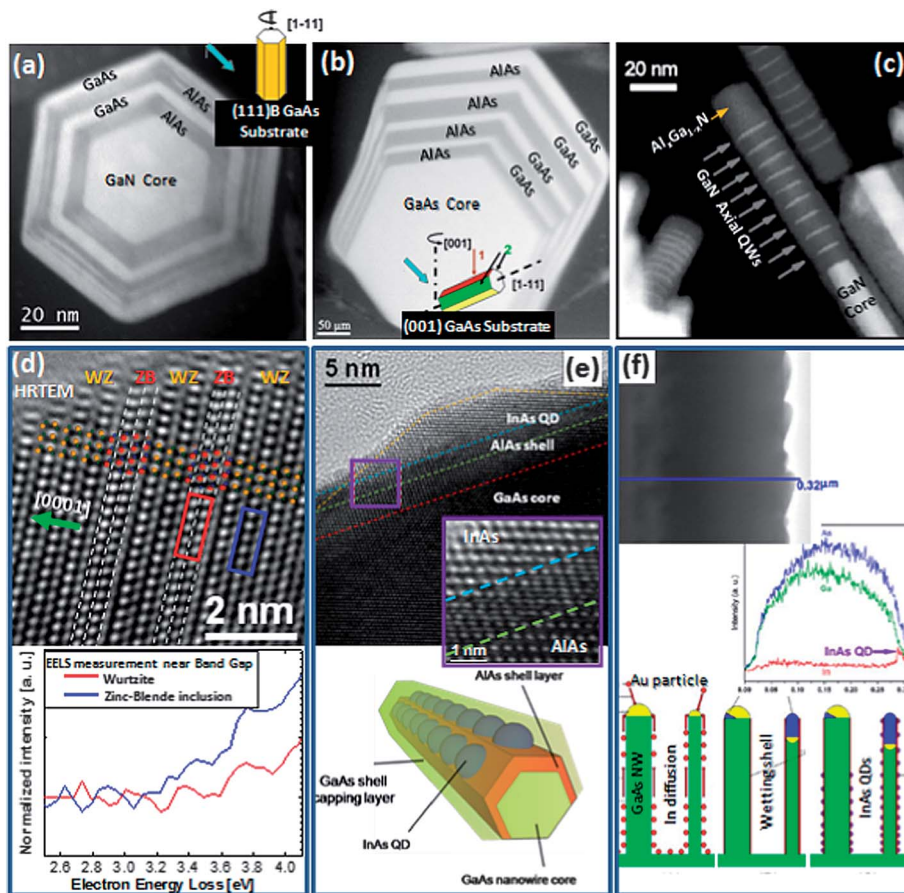


Fig. 1 (a) Radial MQWs in a multishell GaAs–AlAs grown on (111)B GaAs. (b) Radial MQWs in a multishell GaAs–AlAs grown on (001)GaAs. (c) Axial GaN QWRs separated by $\text{Al}_x\text{Ga}_{1-x}\text{N}$ barriers in GaN– $\text{Al}_x\text{Ga}_{1-x}\text{N}$ NWs. Copyright 2011 by the American Physical Society.³¹ e-Tomography HAADF STEM reconstructed models of the radial and axial QWs can be also found elsewhere.^{29,33} (d) ZB domains within a WZ GaN NW, acting as QWs. Adapted with permission from ref. 92. Copyright 2010 American Chemical Society. (e) InAs QD on the surface of a {110}-faceted GaAs–AlAs NW. Adapted with permission from ref. 93. Copyright 2012 American Chemical Society.

in Fig. 1, where we present different types of QWs: radial (also known as coaxial or prismatic) (Fig. 1a and b), axial (Fig. 1c), and polytypic (Fig. 1d), as well as several examples of QDs in a NW (Fig. 1e and f).

II 2D quantum confinement within a nanowire

Nanowires are filamentary crystals with a tailored diameter ranging between a few and ~ 100 – 200 nm. With few exceptions,³⁰ the diameter of the nanowire is often too large for the observation of quantum confinement effects. Still, it is possible to modulate the nanowire composition to obtain nanostructures within the nanowire that show quantum confinement effects. In a quantum well, charge carriers are confined in one spatial direction and free to move in the other two. In principle, quantum wells in nanowires can be obtained directly on the nanowire facets or along the nanowire axis (if the diameter is large enough so that there is no lateral confinement).^{3,31} Such complex nanowire heterostructures have been obtained by combining materials radially and axially along the growth direction of the nanowires.^{32,33} The synthesis starts by

growing a nanowire as a template for further composition modulation in the radial or axial directions with the purpose of confining the carriers in one of them. A precise control of the growth processes is needed to create the desirable heterostructures. In the following, we show examples of these structures inserted in a nanowire, which are characterized by a reduced dimensionality and their improved optical properties.

IIA Radial quantum wells

As the first example of quantum wells in a nanowire we will take into account those heterostructures grown radially on the facets of the wires, creating homogeneous flat shells along their entire length.³⁴ For instance, in the case of growth on the nanowire facets by molecular beam epitaxy, the orientation of the NWs with respect to the molecular beam flux determines the thickness and symmetry of the heterostructures.^{32,33} Using (111)B GaAs as the substrate, vertical NWs are obtained (see Fig. 1a), while other substrate orientations, *i.e.* (001) GaAs, lead to the growth of tilted NWs with respect to the substrate surface (see Fig. 1b).^{35–37} In the first case completely conformal coating of the wires was obtained, while in the second case the structures were asymmetric. In the

latter case and as shown in Fig. 1b, the two top facets receive most of the flux and are therefore the thickest, while the ones facing the substrate have a thickness of almost zero.³³ Still, even in the case where the NWs grow normal to the substrate, inhomogeneities along the wire can occur. Optimization of the growth temperature and molecular fluxes is necessary to achieve uniform shell thickness. The optimal samples are found by performing luminescence spectroscopy along the nanowire axis.³³ At 4.2 K intense emission from the radial QWs at 1.55 eV was observed. This emission was found to extend homogeneously along the major part of the NW length. The full width at half maximum (FWHM) of the PL emission for the QWs was around 5 meV, demonstrating the high quality of the QWs.

These radial heterostructures forming quantum wells are very interesting from the point of view of basic research of quantum physics, as they offer improved physical properties. Already in 2005, the first core-multishell nanowire heterostructures (consisting of a *n*-GaN NW core and $\text{In}_x\text{Ga}_{1-x}\text{N}/\text{GaN}/\text{p-AlGaIn}/\text{p-GaN}$ shells) could be synthesized and used as building blocks for multicolor high-efficiency light-emitting diodes.³⁴ In addition, by controlling the QW thickness on the same heterostructures, wavelength-controlled lasers³⁸ and other optical devices³⁹ such as photodetectors⁴⁰ could be designed. Theoretical studies performed on similar heterostructures as those presented in Fig. 1a³² showed that the multishell overgrowth of a free-standing nanowire, together with its prismatic symmetry, may induce quantum confinement of carriers in a set of quasi-1D quantum channels corresponding to the nanowire edges.⁴¹ In fact, it has been reported theoretically that the electron and hole gases in a radial heterojunction formed in a GaAs-AlGaAs core-multi-shell nanowire can be tuned to different localizations and symmetries inside the core as a function of the doping density/gate potential.⁴² Bertoni *et al.*⁴² demonstrated that contrary to planar heterojunctions, conduction electrons do not form a uniform 2D electron gas (2DEG) localized at the GaAs-AlGaAs interface, but rather show a transition between an isotropic, cylindrical distribution deep in the GaAs core (low doping) and a set of six tunnel-coupled quasi-1D channels (quantum well tubes) at the edges of the interface (high doping). At low doping, these structures should present an additional localization pattern with six separated 2DEG strips. The theoretical studies demonstrated that single 2DEGs at one interface or multiple quasi-1D channels should

form as a function of voltage intensity, polarity, and carrier type.⁴² In this way, Fickenscher *et al.* have demonstrated experimentally the presence of 6 quantum well tubes on the edges created at the intersection between the radial quantum wells in hexagonal prismatic GaAs-AlGaAs core-multishell nanowires, exhibiting extremely high quantum efficiency and intense emission.⁴³ Moreover, coupled plasmon-phonon modes have been observed in quantum well heterostructures similar to those shown in Fig. 1b. In this latter case, a high-density plasma within the quantized structures could be created, opening the possibility for these heterostructures to be used for the confinement of high density of charge in improved nanowire systems.⁴⁴

IIB Axial quantum wells

A second type of quantum wells can be obtained by combining different heterostructures axially, along the NW growth axis, instead of radially. These axial heterostructures have been grown mostly in GaN-based NW templates, using either $\text{In}_x\text{Ga}_{1-x}\text{N}$ ^{45–47} or $\text{Al}_x\text{Ga}_{1-x}\text{N}$,^{48–51} alternatively to obtain the proposed multi- or single quantum well systems (although there are a few exceptions such as those based on $\text{In}_x\text{Ga}_{1-x}\text{As}$).⁵² In this way, multicolor luminescence could be obtained from InGaIn quantum wells grown over GaN nanowire arrays,⁴⁵ or quantum emitter superlattices could be created by alternating GaN and AlN within the same NW.⁵¹ In addition, further bandgap modulation can be achieved by substituting the AlN barriers by a combination of $\text{Al}_x\text{Ga}_{1-x}\text{N}$. In this latter case, as we will see in the following, depending on the Al concentration and growth conditions, a higher blue shift can be obtained.

Axial GaN QWs or nanodiscs (NDs) spaced by $\text{Al}_x\text{Ga}_{1-x}\text{N}$ ($x = 0.08\text{--}1$) barriers were obtained by a stepped process (see Fig. 1c). The synthesis starts by the growth of the GaN cores, faceted by six $\{10\bar{1}0\}$ planes, and is followed by the introduction of Al in the growth process leading to $\text{Al}_x\text{Ga}_{1-x}\text{N}$ sections. Then, the Al flux is cut nine times, thereby creating a nine-fold GaN ND structure. Depending on the growth conditions of the $\text{Al}_x\text{Ga}_{1-x}\text{N}$ barriers, the growth is not strictly axial. The simultaneous radial growth encapsulates the GaN discs and inhibits the release of radial strain. Thus, NDs are under compressive strain, which is reflected in their optical properties.³¹ As the NW widening is progressive along the ND structure, there are strong variations of

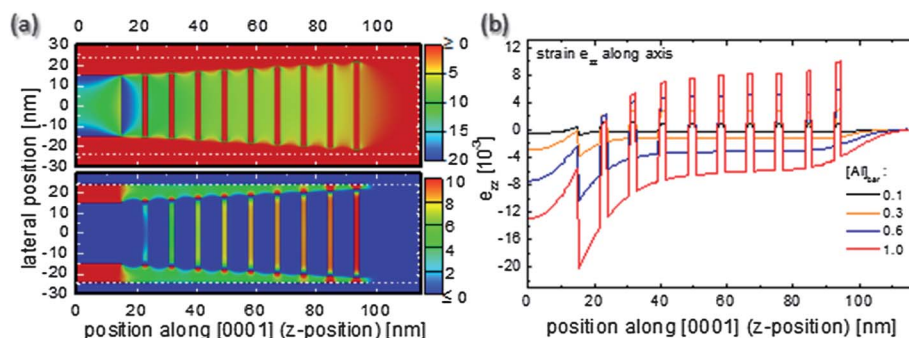


Fig. 2 (a) e_{zz} component for the strain tensor in the case of AlN barriers. Dotted white lines show the NW border. (b) e_{zz} strain along the NDs for different Al concentrations in the barriers. Copyright 2011 by the American Physical Society.³¹

the strain inside the NDs, as shown in the simulation of Fig. 2a. The NDs closer to the base are surrounded by a thicker AlN-shell than those in the tip. As a consequence, the axial strain is higher close to the base and is reduced along the GaN core. The strength of this effect also depends on the Al-content in the barriers. Increasing the Al concentration, the axial strain differences along the NDs embedded in one NW are increased compared to NWs with lower Al in the barriers, as shown in Fig. 2b and evidenced by the results reported in ref. 49. The maximum emission energy of the NDs was found for an Al barrier content of 0.34, reaching 3.73 eV, for subsequently dropping down to 3.69 eV in the case of pure AlN barriers. In agreement with the increase of the strain, the ND emission broadens when the Al-content in the barriers is increased. Also the emission of the GaN core (at 3.48 eV) widens with increasing Al-concentration at the barriers, although its emission energy is not affected. Understanding the optical properties requires taking into account not only the band offset and geometrical factors of the structures, but also the effects of strain relaxation, polarization-induced internal electric fields and surface band bending. Extending the study through calculations and simulations showed the strong influence of the shell thickness on the confinement potential. The emission intensity of the NDs is enhanced for intermediated Al content since it corresponds to a flat-band within the NDs, where the lateral electrical fields are the lowest possible. Time resolved-photoluminescence (TR-PL) experiments result in the suppression of the excitonic character of the emission for high Al concentrations in the barrier due to carrier separation by strain-induced lateral internal electric fields.³¹

IIC Crystal phase engineering: homostructured quantum wells

The nanowire morphology has enabled a new approach of bandgap engineering. The large surface-to-volume ratio enables the formation of crystalline phases otherwise not possible in the bulk (*e.g.*: wurtzite (WZ) and zinc-blende (ZB) phases alternatively, or other twin-based polytypes).^{53–55} In semiconductor materials, most of these twin-based polytypes have a semiconductor behavior, although they present slight changes in the electronic band structure and energy gap (see Table 2).^{53,56} Thus, by combining polytypic phases in one same nanowire, a new type of quantum homostructure may be formed.^{56–58} In an extreme case where the periodicity of defects is perfectly controlled, one finds the so-called twinning superlattices.^{59–61} In this way, Caroff *et al.*⁶⁰ reported the intentional modulation of the crystalline phase in the case of InAs NWs by controlling the growth temperature and their final diameter, to create highly

reproducible twinning superlattices. The twin periodicity was related to the NW diameter as shown in the plot of Fig. 3a and the SEM image included in Fig. 3b. Parallely, doping of the NWs has been also shown to be an efficient alternative to controllably create polytypes in III–V NWs (*e.g.*: in InP).⁶¹ In the absence of Zn during growth, the InP NWs grow with a WZ structure with some randomly spaced stacking faults. However, the growth in the presence of Zn results in the formation of pure zinc-blende domains, thus allowing the design of twinning superlattices when alternating doped and undoped axial sections, as shown in Fig. 3c and d. Notice how the contrast changes at every twin boundary, making the domain's distinction straightforward to a naked eye, due to the enhanced phase contrast obtained in the TEM when imaging the NWs slightly off-axis ($\sim 1^\circ$).⁶² Moreover, Algra *et al.*⁶¹ also reported a comprehensive explanation for the final zigzag NW side facets in the twinned zinc-blende structures, which depends on the contact angle of the catalytic droplet during the vapor-liquid-solid (VLS) growth method employed.

Fig. 1d shows the details of a GaN nanowire containing 2 sections of zinc-blende in a wurtzite matrix. This kind of homostructure has similar characteristics as quantum wells. In the case of GaN, wurtzite and zinc-blende phases form a type II heterojunction, where confinement is achieved just for one type of carriers. In addition, this quantum confinement is possible due to the small size (axial height) of the insertions and because of the dependence of the band structure with respect to the crystalline phase. This is observed in many other semiconductors such as GaAs, Si, InP and GaN depending on the crystalline phase (cubic or hexagonal).^{56,64–66} Often, the transition from one crystal phase to the other is preceded by the presence of twin planes or stacking faults. Stacking faults and twin planes alter the stacking sequence in ZB and WZ structures by omission of one atomic plane at every stacking fault. In the twin boundaries case, each defect rotates the structure by 180° , changing the stacking sequence from the cubic phase to the hexagonal (or inversely) phase where the twin is placed. If the twins are repeated in a periodical way, different polytypes are formed.

For instance, as we have seen above, by controlling the presence of the twin-based defects or inducing them in a controlled way (*i.e.*, by selectively doping the different NW sections during growth), we can perform accurate crystal engineering and obtain the desired superlattice stacking, thus allowing us to induce a predesigned bandgap modulation in our NW systems.⁶⁷ In a previous work,⁶⁷ we showed the way to introduce ZB axial domains in WZ GaN NWs. In this case, by highly doping the NWs with Mg atoms, we obtained the formation of triple twin stacking domains consisting of insertions of 4 ZB monolayers within the WZ structure. These triple twin domains, with barely 2 nm axial heights, extended along the whole width of the NW, creating perfect axial quantum wells. An ensemble of these highly Mg-doped GaN NWs is shown in Fig. 3e. One of the triple twin domains is displayed in the atomic resolution HAADF STEM image in Fig. 3f, where the 3 consecutive twins forming the QW are displayed with green dashed lines. Both ZB and WZ modeled structures are superimposed to the image. The bandgap red-shift achieved exactly

Table 2 Bandgap values in eV for the most common semiconductor in both crystalline phases, wurtzite⁶³ and zinc-blende

Crystalline phase	Material						
	GaN	AlN	GaAs	AlAs	InAs	InP	Si
Zinc-blende	3.3	5.3	1.51	2.35	0.35	1.34	1.12
Wurtzite	3.5	6.2	1.50	1.97	0.48	1.47	0.85

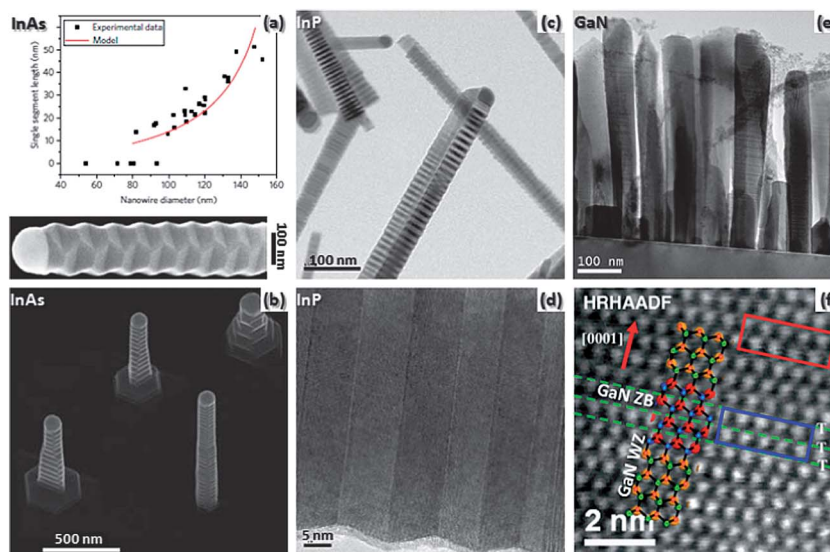


Fig. 3 Crystal phase engineering in a nanowire: homostructured quantum wells. (a and b) In the InAs case reported by Caroff *et al.*,⁶⁰ the twinning periodicity is related to the NW diameter, and can be tuned by controlling the growth temperature. Reprinted with permission from ref. 60. Copyright 2009 American Chemical Society. (c and d) InP NWs where the polytypic control is achieved through Zn doping. Reprinted with permission from ref. 61 and 60. Copyright 2008 American Chemical Society. (e and f) Polytypic GaN NWs. ZB axial phase domains appear when introducing high density of Mg doping atoms during growth. In this latter case, the ZB domains were composed of a triple twin stack in the WZ structure, as observed in the atomic resolution HAADF STEM image in (f). Reprinted with permission from ref. 67 and 60.

within the triple twin domain with respect to the WZ GaN could be measured with high spatial resolution for the first time by Arbiol *et al.*⁶⁷ The precise bandgap measurements were performed in a cold field emission gun (cold-FEG) aberration corrected dedicated STEM by means of low loss electron energy loss spectroscopy (EELS). The bandgap was measured precisely on both, the ZB defect domain and outside in a neighboring WZ area, finding a red-shift of 0.2 eV between both measured bandgaps (the expected 3.4 eV for the WZ area and 3.2 eV in the triple twin domain), in good agreement with the DFT simulations.⁶⁷ An analysis of the optical properties of ZB inclusions in an undoped GaN NW has been reported in ref. 68.

III 1D Confinement in a nanowire: quantum wires

The particular geometry of nanowires has enabled optical experiments that were unthought of with classical thin film structures. For example, if thick enough, they can act as extremely small waveguides.^{69,70} If thin enough, in the range of a quantum wire (QWR), the light emission is extremely bright thanks to the suppression of the total internal reflection.⁷¹ As a consequence, NWs are currently considered as ideal elements for ultra-bright light emitting diodes (LEDs) and single photon sources.^{72–74} In the literature there are many reports regarding semiconductor quantum wells and quantum dots, but only a few articles focus on the synthesis of self-assembled quantum wires (QWRs) on NWs. Most of the reports on QWRs employ chemical solution synthesis for different materials^{75–79} obtaining single QWRs with a variety of diameters. GaAs,⁸⁰ InGaAs⁸¹ or ZnO^{82,83} have also been successfully synthesized as QWRs self-assembled in bulk materials or on surfaces by molecular beam epitaxy (MBE). Furthermore, although QWRs have been widely

studied theoretically since the early 20s of the last century (at the beginning of electronics)^{84–86} and later on grown on bulk surfaces or layers,^{87,88} few works integrate this 1-dimensional (1D) quantum structure in a nanowire. By inserting quantum structures in the nanowire waveguides, their brightness can be increased by up to an order of magnitude compared to self-assembled quantum structures on a planar substrate.

In the particular case of GaN, self-organized GaN QWRs could be only obtained previously as core elements in GaN–AlGaIn core-shell NWs.⁸⁹ Recently, axial III–V QWRs could be grown for the first time in a self-assembled growth mode on the edges of nanowires. Our research on the material showed that GaN QWR formation within a NW was a consequence of a self-limited pseudomorphic growth.⁹⁰ Along this section, we are going to focus on that work, which presents a new approach for bandgap engineering consisting in the growth control of GaN quantum wires (QWRs) on the 6 vertices of hexagonal prismatic GaN–AlIn core-shell nanowires, acting as templates. As a consequence of the nanowire geometry, the self-assembled QWRs are obtained directly on the nanowire edges.^{31,90}

The GaN–AlIn core-shell NWs were first grown by the catalyst-free plasma assisted molecular beam epitaxy (PAMBE).³¹ The first synthesis step forms the GaN cores as the template for the entire NWs. Initially the GaN basis of the NWs was obtained with lateral faceting on the $\{1\bar{1}00\}$ planes, having diameters of 25–50 nm and lengths ranging from 130 nm to 300 nm. The unidirectional growth along the *c*-axis was promoted using a nitrogen-rich environment. Then, an axial segment of AlN was deposited, and due to its finite lateral growth rate radially covered the lateral $\{1\bar{1}00\}$ facets of the GaN core. This step resulted in the additional formation of six $\{1\bar{1}\bar{2}0\}$ AlN planes, which might differ in geometric extension, at the intersections between every two $\{1\bar{1}00\}$ facets (truncated edges). After that,

self-assembly of GaN QWRs was possible on these $\{1\bar{1}20\}$ edges with simultaneous formation of an axial GaN segment on the top of the wire.

The GaN nucleation occurred exclusively at the AlN $\{1\bar{1}20\}$ facets and no lateral deposition on the $\{1\bar{1}00\}$ planes of the AlN shell was found. The QWRs were then created on the 6 $\{1\bar{1}20\}$ edges, and extended axially along the $[000\bar{1}]$ NW growth axis with *N*-face polarity (with top surfaces terminated with N atoms).³⁷ It was observed that the GaN deposited at those sides was easily damaged under the electron beam. In order to prevent beam damage, a final AlN shell covering the entire structure was deposited employing the lateral growth of AlN. Deposition of the AlN external shell led to an enhancement of the GaN QWRs stability and a suppression of PL quenching, allowing a better quantum confinement.

Representative high-angle annular dark field (HAADF) or Z-contrast images of the NWs are shown in Fig. 4a–c at different magnifications. Notice the change in the HAADF intensity when imaging the different regions of the NWs due to their different compositions, which allows the direct identification of the GaN and AlN regions. The GaN has brighter intensity under Z-contrast imaging conditions since its constituents are heavier than the AlN ones (*i.e.*, $Z_{\text{Ga}} = 31$ while $Z_{\text{Al}} = 13$). Besides distinguishing the GaN core from the AlN barriers, bright lines at the NW edges are also observed upon closer inspection, corresponding to the presence of the GaN QWRs (Fig. 4b and c) nucleated on the $\{1\bar{1}20\}$ AlN facets. The lateral size of the QWRs ranges between 1 and 10 monolayers in projection. The atomic resolution image in Fig. 4c clearly shows 2 projected $\{1\bar{1}00\}$ planes along the length of the NW, belonging to a GaN QWR. A

transversal intensity profile across the wire reveals the different material compositions superimposed on the NW thickness background, leading to the half-hexagon shape in Fig. 4d. A 3D model of the structure is included on the right side of the figure, showing several views of the heterostructure.

Photoluminescence analyses performed on these novel 1D quantum systems showed two different emission bands. The first was found at about 3.5 eV (see the inset in Fig. 5a), corresponding to the GaN base emission, which is blue shifted by the presence of the AlN shell which compresses the core. The second emission band was attributed to the presence of the QWRs, appearing in the range 3.85–4.05 eV, which was shifted to higher energies (0.5 eV higher) because of the strong quantum confinement in the QWR. Low-temperature time-resolved PL measurements performed at different excitation energies did not show changes in the emission energy attributed to the QWRs, demonstrating that those emissions should correspond to the confinement of non-polar surfaces, in good agreement with the QWRs grown on the $\{1\bar{1}20\}$ edges. In order to get further insight about the emission from individual QWRs, μ -PL measurements were performed on individual NWs as shown in Fig. 5a. Several narrow emission lines were found for each NW, corresponding to the emission from the different QWRs. As mentioned before, there is a spread of sizes that results in different energy emission depending on the wire diameter, as also corroborated by the simulations performed. This energy dependence of the emission with the diameter was calculated as shown in Fig. 5b, where a histogram of the QWR energy emission for 24 NWs experimentally measured is also displayed. In addition spatially resolved *in situ* optical

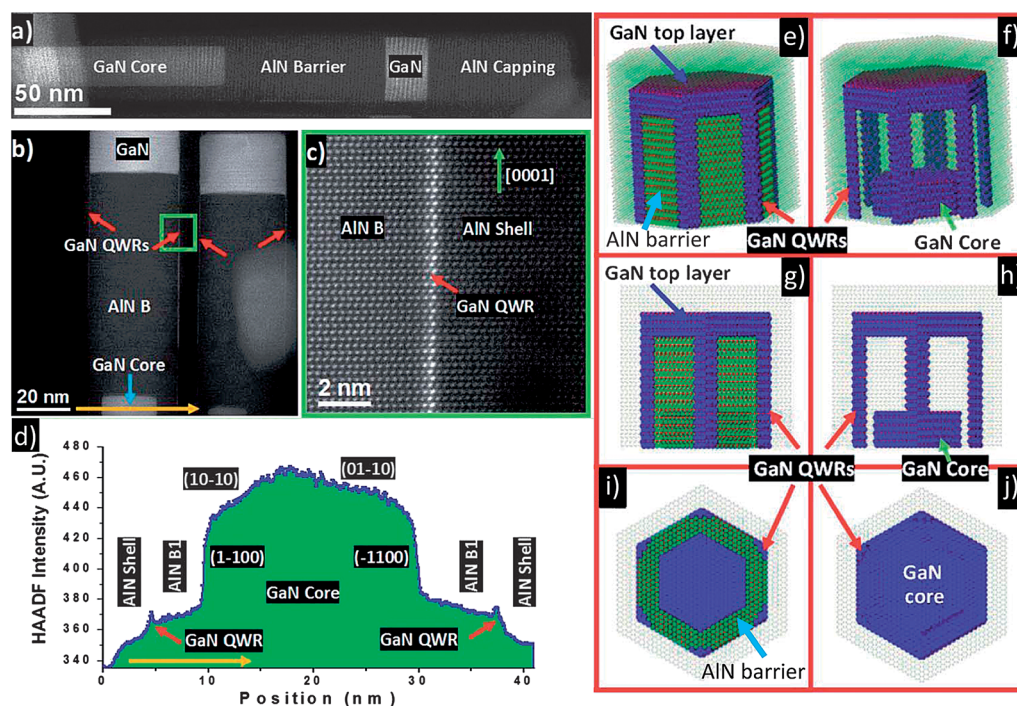


Fig. 4 (a–c) HAADF images of the GaN–AlN NWs, presenting GaN QWRs at the corners of the NW. (d) Intensity profile revealing the NW cross-section morphology. (e–j) 3D model of the studied structure. Reprinted with permission from ref. 90. An animated movie of the previous models can be also found elsewhere.⁹¹

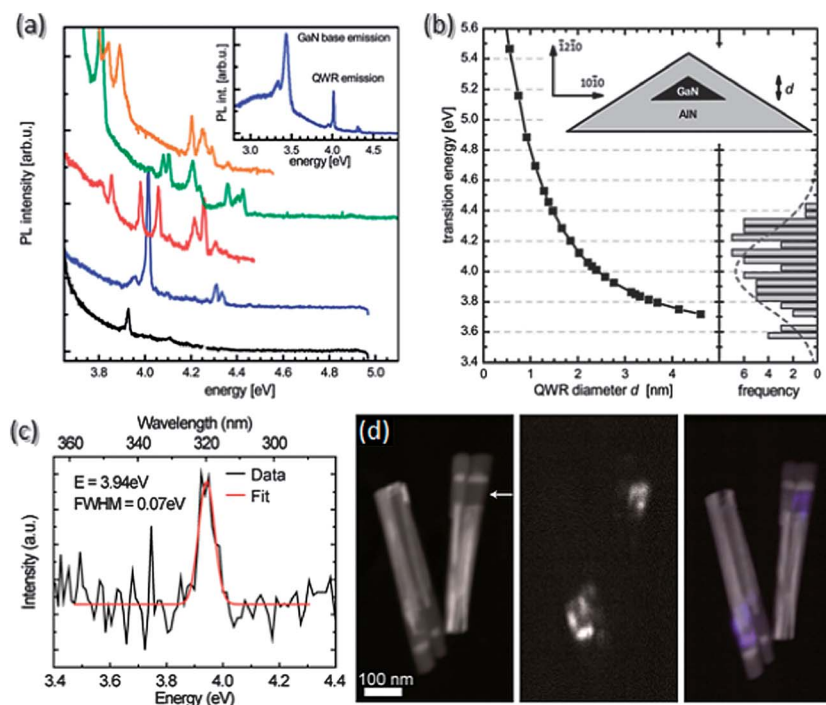


Fig. 5 (a) Low temperature PL spectra from single GaN-AlN NWs where the peaks are due to GaN QWRs. (b) Calculated energy emission of the QWRs as a function of its diameter (left panel). At the right side is included the experimental histogram. The experimental averaged QWR diameter is comprised between 1.7 and 2.5 nm. (a and b) Reprinted with permission from ref. 90. (c) Low temperature (93 K) CL spectrum from the individual NW marked with a white arrow in (d), showing a narrow peak (FWHM = 0.07 eV) at 3.94 eV (by Gaussian fitting). (d) 1st panel: STEM image; 2nd panel: corresponding panchromatic CL image, 3rd panel: false colored overlay from 1st and 2nd panels.

measurements for these quantum structures obtained by cathodoluminescence (CL) in a STEM are presented in Fig. 5c and d. In this case we can clearly see that the QWRs show strong CL intensity centered at 3.94 eV (Fig. 5c), significantly stronger than the emission from the GaN cores (Fig. 5d). It is also evident that the QWR emission is only observed on the lower AlN segment. The top AlN segment was formed during the growth of the capping layer, *i.e.* no QWRs are present on the side facets of this part. The energy of the CL emission line corresponding to QWRs is consistent with μ -PL results, while the 70 meV FWHM is limited by the resolution of serial-mode CL collection by the photomultiplier tube. Together, μ -PL and CL results confirm the high structural and optical quality of these newly developed quantum structures.

IV 0D confinement in a nanowire: quantum dots

Until now, we have seen how carriers can be trapped in two and one dimensions in a nanowire respectively by the formation of QWs and QWRs. It is possible to go one step further and confine the carriers in all three spatial dimensions, by creating a quantum dot (QD), considered as a 0 dimensional structure. In the following we present some examples of QDs in NWs, distinguishing between those QDs grown by following the Stranski-Krastanov mechanism and those obtained by self-induced diffusion processes.

IVA Quantum dots generated by the Stranski-Krastanov process

Recently, new methods to grow quantum dots in nanowires by embedding them on the facets and edges have been reported.^{92–94} In those works, the decoration of GaAs nanowire facets with InAs quantum dots (QDs) was demonstrated. As commented before, GaAs NWs usually grow along the [111]B zone axis and present hexagonal sections, normally faceted either by {110}³² or {112}⁹⁵ planes, depending on the synthesis method employed.

Thus, using the catalyst-free gallium assisted method,⁹⁶ {110} GaAs faceted NWs were obtained. Stranski-Krastanov (SK) InAs QDs do not form on {110} facets of GaAs due to the unfavorable interface energy. In order to promote the formation of QDs, the facets have to be covered with a thin layer of AlAs^{97–99} (see Fig. 1e). In Fig. 1e, we show a high resolution TEM (HRTEM) image of an InAs QD placed on the edge of a GaAs-AlAs core-shell NW. Notice that both the GaAs-AlAs and AlAs-InAs interfaces can be observed in the HRTEM image. The HRTEM inset in Fig. 1e shows the superposition of InAs and AlAs layers.⁹² Further HRTEM cross-sectional inspections confirmed that the QDs are partially buried in the AlAs shell, as shown in Fig. 6a and b. This fact indicates that the QD formation involves InAs diffusion in the (110) AlAs along a few monolayers, as an essential part of the QDs creation on the {110} facets.⁹² The InAs QDs were modeled as 5 nm height truncated pyramids, discretely embedded on the facets and

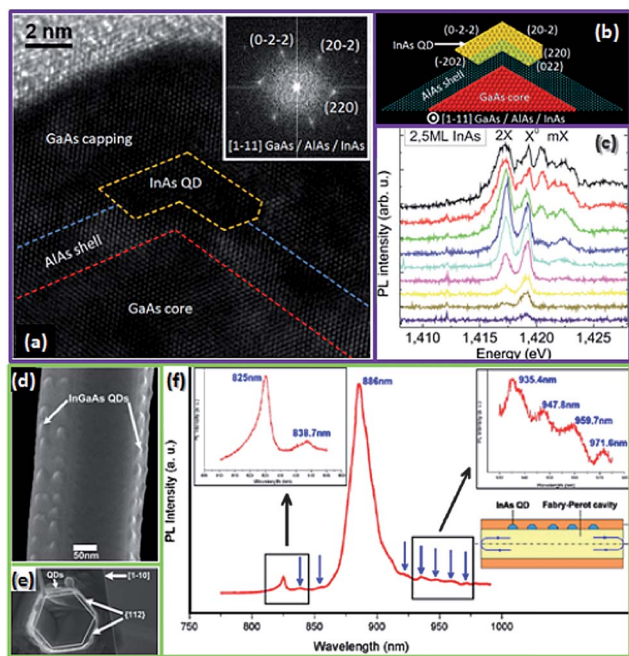


Fig. 6 The top panel (violet squared) shows a TEM image of an InAs QD in a {110} GaAs@AlAs NWs, partially buried in the AlAs shell (a) within a 3D atomic model (b). The PL measurements performed at different excitation powers (c) revealed the excitation of single and biexcitons in the QD. Reprinted with permission from ref. 92. Copyright 2010 American Chemical Society. In the bottom panel (marked in green) are displayed a couple of SEM images (d and e) of {112}GaAs NWs, showing facets plenty of QDs. The PL spectrum corresponding to the InGaAs QDs visualized in (d) and (e) is included in (f). (d and e) Reprinted with permission from ref. 102. Copyright 2012, American Institute of Physics. (f) Reprinted with permission from ref. 93. Copyright 2012 American Chemical Society.

edges of the GaAs NW core.⁹² The shape and distribution of the SK quantum dots embedded on the surface (facets and edges) of a nanowire have been recently theoretically predicted and calculated. It was found that their shape and distribution directly depend on the surface and elastic energies between both the surface material and QD.¹⁰⁰ The theoretical results show a direct relationship between the nanowire diameter and the final morphology of the developed QD structures, which is in good agreement with the experiments reported by other authors. In this way, for thinner NWs only the formation of surface nanorings (circling the whole NW external perimeter) would be allowed. When NWs overcome a critical size, the formation of QDs on the facets would be then allowed. When exceeding the next NW diameter threshold the QDs would be created on the NW edges. Finally, when the NWs are thick enough the formation of QDs in both, facets and edges, would take place.¹⁰⁰

To probe the nature of the optical emission in these QD structures, PL measurements were performed as a function of the excitation power. In Fig. 6c the PL intensity for the different excitation power is displayed. The peak at 1.419 eV varied linearly, corresponding to a single exciton (X^0), while the peak at 1.417 eV varies with excitation power in a quadratic way, indicating the presence of double excitons (2X). At higher energies multiexcitonic (mX) recombination lines were also detected. All

together were in good agreement with the presence of relatively good quality InAs QDs.

InGaAs SK QDs were also obtained by the metal organic vapor chemical deposition (MOVCD) method. In this case, the GaAs NWs exhibited {112} facets.^{93,95,101,102} In contrast to the {110} faceted NWs, the QD formation in {112} surfaces is thermodynamically allowed (see Fig. 1d and e) without the need for intermediate layers (e.g.: AlAs). In addition, the InAs deposition time and the diameter of the wires were found to have considerable impact on the final quality of the QDs coverage. In principle, in thicker NWs the QD formation was easier since less In atoms are needed to form the initial wetting shell, necessary to assure a SK growth. However, when the NW diameters exceeded a critical size (e.g.: 250 nm), the NWs were only partially covered by QDs, as the wetting layer could not cover the entire NW surface. Controversially, by increasing the InAs deposition time the QDs started to coalesce. In Fig. 6e and f we show two examples of InGaAs QDs embedded on {112} GaAs facets, with $\text{In}_{0.7}\text{Ga}_{0.3}\text{As}$ and $\text{In}_{0.9}\text{Ga}_{0.1}\text{As}$ QD stoichiometry, respectively.¹⁰² As in the previous example, an extra GaAs shell was deposited on top of the QDs to protect them from oxidation and assure a better quantum confinement. Their optical characterizations were performed by means of PL measurements, resulting in emission peaks in the range of 857–930 nm. The PL spectrum included in Fig. 6f corresponds to a sample containing GaAs NWs with pure InAs QDs. The narrow peak at 825 nm is due to the GaAs NW, and the one at 886 nm is related to the presence of the InAs QDs. Resonant peaks in the spectrum indicate the formation of a Fabry-Perot cavity in the GaAs NW. As a result, in these structures, the light production came from the QDs and the cavity was formed by the NW, meaning that they were decoupled.

IVB Quantum dots obtained by self-induced diffusion processes

Another new approach has been recently proposed for the growth of QDs self-assembled to NWs. This is the case reported by Heiss *et al.*¹⁰³ where self-assembled QDs were obtained from the synthesis of core-shell GaAs-AlGaAs NWs. Once again, the efficiency of photon extraction in quantum structures (QDs) self-assembled in a nanowire is dramatically enhanced with respect to the efficiency of the QDs contained in bulk materials. In a recent paper, we have presented the self-assembled formation of $\text{Al}_{0.1}\text{Ga}_{0.9}\text{As}$ QDs covered by an $\text{Al}_{0.6}\text{Ga}_{0.4}\text{As}$ layer inside the $\text{Al}_{0.33}\text{Ga}_{0.67}\text{As}$ shell of the NW. The QD formation was promoted by the different Ga and Al mobilities on the surface of the NWs, resulting in Al segregation to form the QD confinement. The whole growth process was reproducible from wire to wire and from growth to growth. Moreover, the QDs obtained were stable and presented excellent optical properties, being very bright even near the surface (detection rate higher than 1 MHz). The cathodoluminescence (CL) measurements, performed in a scanning electron microscope (SEM), revealed two different emission energies: a broad band emission spatially continuous coming from the core at approximately 820 nm and a discontinuous emission line along the NW at higher energy (677 nm) corresponding to the presence of QDs, acting as

extremely localized emitters.¹⁰³ PL analyses were also performed, in order to characterize individual QDs, showing sub-100 μ eV linewidths as the general trend. The electronic states of the system were found to be oppositely ordered relative to the Stranski–Krastanov QDs, where the higher energy belongs to the matrix. Instead, here, the GaAs layers form the lowest energy edge existing states at higher energy which confines the QD.¹⁰³

The procedure started by the growth of the GaAs cores of the NWs on a (111) Si substrate.¹⁰⁴ Then, the conditions were changed to allow the lateral growth of the $\text{Al}_x\text{Ga}_{1-x}\text{As}$ shells with two different Al contents, $x = 33\%$ or 51% (the $\text{Al}_{0.33}\text{Ga}_{0.67}\text{As}$ shells were alternated with 20 nm GaAs quantum wells). The QD-in-a-nanowire system was created by the formation of inhomogeneities in the shell. Empirical observations of the structures were performed using the Z-contrast STEM technique through an aberration corrected microscope. The different axial layers with compositional changes could be distinguished with naked the eye when analyzing the cross-section samples after imaging them at atomic resolution. As was explained in Section III, the darker the observed region, the lower the Z of the observed area (the higher Al content), *i.e.*, the brighter area in the center of the NW corresponds to the GaAs composition (no

Al is present in the core). Fig. 7 shows the formation of radial dark stripes emerging from the core corners in the $\text{Al}_x\text{Ga}_{1-x}\text{As}$ regions following the $\{110\}$ directions, which are often opened in a Y-shape along two $\{112\}$ planes near the outer surface of the NWs. The inside volume containing lower Al content corresponds to the QD structure, which is surrounded with this Al-rich covering (see Fig. 7d where the Al-rich plane is the $(10\bar{1})$ and it is split along the $(1\bar{1}2)$ and $(2\bar{1}1)$, and a further (121) plane closes the structure). A simple 3D atomic model was created to illustrate the morphology of the QDs; however, new models are required taking into account the outer evolving shells that cover the entire QDs. In future works we will deal with more sophisticated models¹⁰⁵ and work on a better understanding of these QD structures' growth mechanisms which are definitively related to self-induced diffusion processes as suggested elsewhere.¹⁰³

V Conclusions

Nowadays, the creation of quantum structures in semiconductor materials has turned into a trend topic for promising technological applications and theoretical research. Thanks to their particular morphology, nanowires offer the three-dimensional modulation of composition and thereby a three-dimensional arrangement of quantum structures. Here we have presented an overview of different quantum structures in-a-wire, going from the QWs to the QDs, passing through QWRs, all embedded in NWs, for the most common binary/(ternary) semiconductor compounds. As a result, high quality quantum emitters and absorbers of great brightness at precise wavelengths have been obtained integrated in NWs. In order to improve the future devices based on integrated quantum structures in-a-nanowire, a perfect control of the nature of the interfaces and the size, morphology and composition of the quantum structures is required. Our initial results are very promising. More work has to be carried out in order to obtain a higher degree of perfection of the quantum structures, translated into even smaller values of the FWHM.

VI Experimental

STEM measurements

Aberration-corrected HAADF-STEM and ABF-STEM were performed on a FEI Titan 60–300 k eV operated at 300 kV. Sample preparation of the as-grown NWs for (S)TEM analyses was performed as follows: first of all the NWs were mechanically removed from the substrate, then transferred to a holey or lacey carbon grid and placed in the microscope, for HAADF-STEM observation.⁵³ Images were analyzed by means of Gatan Digital Micrograph software. In addition, 3D atomic supercell modeling was performed by using the Rhodius software package,¹⁰⁶ which allows creation of complex atomic models,^{107,108} including nanowire-like structures.^{109,110}

Cathodoluminescence

Spatially resolved cathodoluminescence studies were performed on a JEOL 2011 TEM/STEM equipped with a Gatan MONOCL3 CL+ system operated at 120 kV. The CL signal was

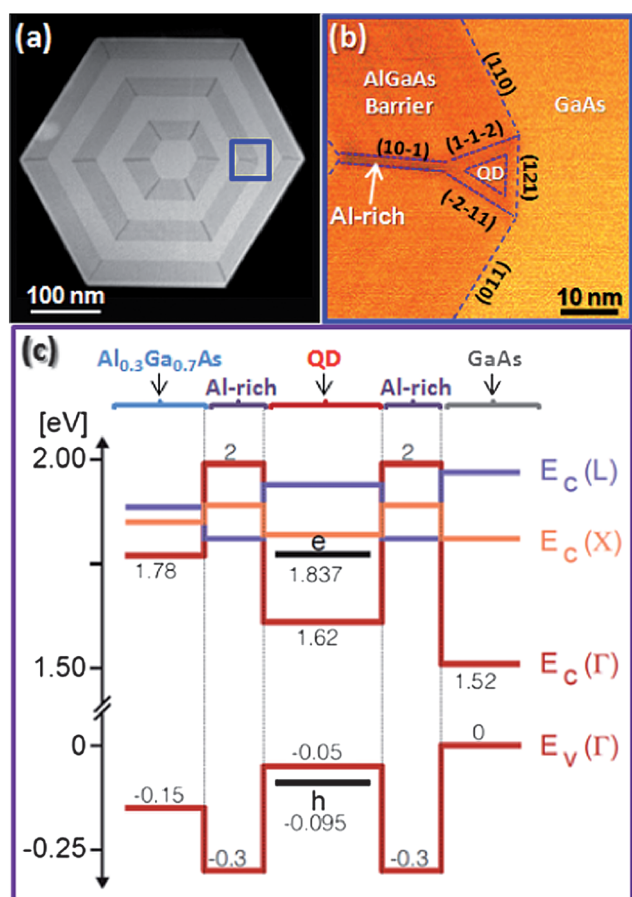


Fig. 7 (a) Cross-section HAADF image of a GaAs@AlGAs NW, squaring the detail amplified and false colored in (b). The false color enhances the contrast, allowing easier distinction of the different composition areas. (c) Band diagram of the system taken from atomistic pseudopotential theory. Reprinted with permission from ref. 103. Copyright 2013.

collected by a high sensitivity photomultiplier tube (HSPMT) for concurrent STEM and CL mapping, and spectrum collection, by busing Gatan Digital Micrograph software. The sample was cooled to 93 K by a liquid nitrogen-cooled cryogenic holder.^{111–113}

Acknowledgements

This work was supported by the Spanish MICINN projects MAT2010-15138 (COPEON) and CSD2009-00013 (IMAGINE), and Generalitat de Catalunya projects NanoAraCat, 2009-SGR-770 and XaRMAE. XZ and SG acknowledge support by the Center for Excitonics, an Energy Frontier Research Center funded by the US Department of Energy, Office of Basic Energy Sciences under Award number DE-SC0001088. MdIM thanks the CSIC JAE Pre-Doc program. AFiM acknowledges funding from SNF through NCCR-QSIT and grant no. 134506.

References

- 1 Y. Cui and C. M. Lieber, *Science*, 2001, **291**, 851–853.
- 2 X. F. Duan, Y. Huang, Y. Cui, J. F. Wang and C. M. Lieber, *Nature*, 2001, **409**, 66–69.
- 3 F. Qian, Y. Li, H. G. Park and C. M. Lieber, *Appl. Phys. Lett.*, 2005, **87**, 173111.
- 4 F. Qian, S. Gradecak, Y. Li, C.-Y. Wen and C. M. Lieber, *Nano Lett.*, 2005, **5**, 2287–2291.
- 5 H. P. T. Nguyen, S. Zhang, K. Cui, X. Han, S. Fatholouloumi, M. Couillard, G. A. Botton and Z. Mi, *Nano Lett.*, 2011, **11**, 1919–1924.
- 6 W. U. Wang, C. Chen, K. H. Lin, Y. Fang and C. M. Lieber, *Proc. Natl. Acad. Sci. U. S. A.*, 2005, **102**, 3208–3212.
- 7 G. F. Zheng, F. Patolsky, Y. Cui, W. U. Wang and C. M. Lieber, *Nat. Biotechnol.*, 2005, **23**, 1294–1301.
- 8 J. Teubert, P. Becker, F. Furtmayr and M. Eickhoff, *Nanotechnology*, 2011, **22**, 275505.
- 9 J. Wallys, J. Teubert, F. Furtmayr, D. M. Hofmann and M. Eickhoff, *Nano Lett.*, 2012, **12**, 6180–6186.
- 10 Y. Cui, Z. H. Zhong, D. L. Wang, W. U. Wang and C. M. Lieber, *Nano Lett.*, 2003, **3**, 149–152.
- 11 C. K. Chan, H. Peng, G. Liu, K. McIlwrath, X. F. Zhang, R. A. Huggins and Y. Cui, *Nat. Nanotechnol.*, 2008, **3**, 31–35.
- 12 C. K. Chan, X. F. Zhang and Y. Cui, *Nano Lett.*, 2008, **8**, 307–309.
- 13 B. M. Kayes, H. A. Atwater and N. S. J. Lewis, *Appl. Phys. A: Mater. Sci. Process.*, 2005, **97**, 114302.
- 14 B. Z. Tian, X. L. Zheng, T. J. Kempa, Y. Fang, N. F. Yu, G. H. Yu, J. L. Huang and C. M. Lieber, *Nature*, 2007, **449**, 885–888.
- 15 C. Colombo, M. Heiß, M. Graetzel and A. Fontcuberta i Morral, *Appl. Phys. Lett.*, 2009, **94**, 173108.
- 16 P. Krogstrup, *et al.*, *Nat. Photonics*, 2013, **7**, 306–310.
- 17 A. I. Hochbaum, R. K. Chen, R. D. Delgado, W. J. Liang, E. C. Garnett, M. Najarian, A. Majumdar and P. D. Yang, *Nature*, 2008, **451**, 163–165.
- 18 A. I. Boukai, Y. Bunimovich, J. Tahir-Kheli, J. K. Yu, W. A. Goddard and J. R. Heath, *Nature*, 2008, **451**, 168.
- 19 C. Thelander, T. Martensson, M. T. Bjork, B. J. Ohlsson, M. W. Larsson, L. R. Wallenberg and L. Samuelson, *Appl. Phys. Lett.*, 2003, **83**, 2052–2055.
- 20 A. Pfund, I. Shorubalko, K. Ensslin and R. Leturcq, *Phys. Rev. Lett.*, 2007, **99**, 036801.
- 21 M. H. M. van Weert, N. Akopian, U. Perinetti, M. P. van Kouwen, R. E. Algra, M. A. Veheijen, E. P. A. M. Bakkers, L. P. Kouwenhoven and V. Zwiller, *Nano Lett.*, 2009, **9**, 1989–1993.
- 22 Y. J. Doh, J. A. van Dam, A. L. Roest, E. P. A. M. Bakkers, L. P. Kouwenhoven and S. De Franceschi, *Science*, 2005, **309**, 272–275.
- 23 M. T. Borgstrom, V. Zwiller, E. Muller and A. Imamoglu, *Nano Lett.*, 2005, **5**, 1439–1443.
- 24 G. Bulgarini, M. E. Reimer, T. Zehender, M. Hocevar, E. P. A. M. Bakkers, L. P. Kouwenhoven and V. Zwiller, *Appl. Phys. Lett.*, 2012, **100**, 121106.
- 25 M. E. Reimer, G. Bulgarini, N. Akopian, M. Hocevar, M. B. Bavinck, M. A. Verheijen, E. P. A. M. Bakkers, L. P. Kouwenhoven and V. Zwiller, *Nat. Commun.*, 2012, **3**, 737.
- 26 F. Glas, *Phys. Rev. B: Condens. Matter Mater. Phys.*, 2006, **74**, 121302.
- 27 N. Skold, L. S. Karlsson, M. W. Larsson, M. E. Pistol, W. Seifert, J. Tragardh and L. Samuelson, *Nano Lett.*, 2005, **5**, 1943–1947.
- 28 M. S. Gudiksen, L. J. Lauhon, J. Wang, D. C. Smith and C. M. Lieber, *Nature*, 2002, **415**, 617–620.
- 29 <http://departments.icmab.es/gaen/model4>.
- 30 A. Myalitsin, C. Strelow, Z. Wang, Z. Li, T. Kipp and A. Mews, *ACS Nano*, 2011, **5**, 7920–7927.
- 31 F. Furtmayr, J. Teubert, P. Becker, S. Conesa-Boj, J. R. Morante, J. Arbiol, A. Chernikov, S. Schäfer, S. Chatterjee and M. Eickhoff, *Phys. Rev. B: Condens. Matter Mater. Phys.*, 2011, **84**, 205303.
- 32 A. Fontcuberta i Morral, D. Spirkoska, J. Arbiol, M. Heigoldt, M. J. R. Morante and G. Abstreiter, *Small*, 2008, **4**, 899–903.
- 33 M. Heigoldt, J. Arbiol, D. Spirkoska, J. M. Rebled, S. Conesa-Boj, G. Abstreiter, F. Peiro, J. R. Morante and A. Fontcuberta i Morral, *J. Mater. Chem.*, 2009, **19**, 840–848.
- 34 F. Qian, Y. Li, S. Gradecak, D. L. Wang, C. J. Barrelet and C. M. Lieber, *Nano Lett.*, 2004, **4**, 1975–1979.
- 35 A. Fontcuberta i Morral, C. Colombo, G. Abstreiter, J. Arbiol and J. R. Morante, *Appl. Phys. Lett.*, 2008, **92**, 063112.
- 36 E. Uccelli, J. Arbiol, C. Magen, P. Krogstrup, E. Russo-Averchi, M. Heiss, G. Mugny, F. Morier-Genoud, J. Nygard, J. R. Morante and A. Fontcuberta i Morral, *Nano Lett.*, 2011, **11**, 3827–3832.
- 37 M. de la Mata, C. Magen, J. Gazquez, M. I. B. Utama, M. Heiss, S. Lopatin, F. Furtmayr, C. J. Fernandez-Rojas, B. Peng, J. R. Morante, R. Rurali, M. Eickhoff, A. Fontcuberta i Morral, Q. Xiong and J. Arbiol, *Nano Lett.*, 2012, **12**, 2579–2586.
- 38 F. Qian, Y. Li, S. Gradecak, H.-G. Park, Y. Dong, Y. Ding, Z. L. Wang and C. M. Lieber, *Nat. Mater.*, 2008, **7**, 701–706.

- 39 R. Koester, J.-S. Hwang, D. Salomon, X. Chen, C. Bougerol, J.-P. Barnes, D. L. S. Dang, L. Rigutti, A. de Luna Bugallo, G. Jacopin, M. Tchernycheva, C. Durand and J. Eymery, *Nano Lett.*, 2011, **11**, 4839–4845.
- 40 A. de Luna Bugallo, G. Jacopin, F. H. Julien, C. Durand, X. Chen, D. Salomon, J. Eymery and M. Tchernycheva, *Appl. Phys. Lett.*, 2011, **98**, 233107.
- 41 G. Ferrari, G. Goldoni, A. Bertoni, G. Cuoghi and E. Molinari, *Nano Lett.*, 2009, **9**, 1631–1635.
- 42 A. Bertoni, M. Royo, F. Mahawish and G. Goldoni, *Phys. Rev. B: Condens. Matter Mater. Phys.*, 2011, **84**, 205323.
- 43 M. Fickenscher, T. Shi, H. E. Jackson, L. M. Smith, J. M. Yarrison-Rice, C. Zheng, P. Miller, J. Etheridge, B. M. Wong, Q. Gao, S. Deshpande, H. H. Tan and C. Jagadish, *Nano Lett.*, 2013, **13**, 1016–1022.
- 44 B. Ketterer, J. Arbiol and A. Fontcuberta i Morral, *Phys. Rev. B: Condens. Matter Mater. Phys.*, 2011, **83**, 245327.
- 45 R. Armitage and K. Tsubaki, *Nanotechnology*, 2010, **21**, 195202.
- 46 M. Wölz, V. M. Kaganer, O. Brandt, L. Geelhaar and H. Riechert, *Appl. Phys. Lett.*, 2011, **98**, 261907.
- 47 J. Lahnemann, O. Brandt, C. Pfüller, T. Flissikowski, U. Jahn, E. Luna, M. Hanke, M. Knellingen, A. Trampert and H. T. Grahn, *Phys. Rev. B: Condens. Matter Mater. Phys.*, 2011, **84**, 155303.
- 48 J. Renard, R. Songmuang, G. Tourbot, C. Bougerol, B. Daudin and B. Gayral, *Phys. Rev. B: Condens. Matter Mater. Phys.*, 2009, **80**, 121305(R).
- 49 L. Rigutti, J. Teubert, G. Jacopin, F. Fortuna, M. Tchernycheva, A. De Luna Bugallo, F. H. Julien, F. Furtmayr, M. Stutzmann and M. Eickhoff, *Phys. Rev. B: Condens. Matter Mater. Phys.*, 2010, **82**, 235308.
- 50 R. Songmuang, G. Katsaros, E. Monroy, P. Spathis, C. Bougerol, M. Mongillo and S. De Franceschi, *Nano Lett.*, 2010, **10**, 3545–3550.
- 51 L. F. Zagonel, S. Mazzucco, M. Tence, K. March, R. Bernard, B. Laslier, G. Jacopin, M. Tchernycheva, L. Rigutti, F. H. Julien, R. Songmuang and M. Kociak, *Nano Lett.*, 2011, **11**, 568–573.
- 52 M. Heiß, A. Gustafsson, S. Conesa-Boj, F. Peiró, J. R. Morante, G. Abstreiter, J. Arbiol, L. Samuelson and A. Fontcuberta i Morral, *Nanotechnology*, 2009, **20**, 075603.
- 53 A. Fontcuberta i Morral, J. Arbiol, J. D. Prades, A. Cirera and J. R. Morante, *Adv. Mater.*, 2007, **2007**(19), 1347.
- 54 J. Arbiol, B. Kalache, P. Roca i Cabarrocas, J. R. Morante and A. Fontcuberta i Morral, *Nanotechnology*, 2007, **18**, 305606.
- 55 A. Mishra, L. V. Titova, T. B. Hoang, H. E. Jackson, L. M. Smith, J. M. Yarrison-Rice, Y. Kim, H. J. Joyce, Q. Gao, H. H. Tan and C. Jagadish, *Appl. Phys. Lett.*, 2007, **91**, 263104.
- 56 D. Spirkoska, J. Arbiol, A. Gustafsson, S. Conesa-Boj, F. Glas, I. Zardo, M. Heigoldt, M. H. Gass, A. L. Bleloch, S. Estrade, M. Kaniber, J. Rossler, F. Peiro, J. R. Morante, G. Abstreiter, L. Samuelson and A. Fontcuberta i Morral, *Phys. Rev. B: Condens. Matter Mater. Phys.*, 2009, **80**, 245325.
- 57 N. Akopian, G. Patriarche, L. Liu, J.-C. Harmand and V. Zwiller, *Nano Lett.*, 2010, **10**, 1198–1201.
- 58 K. Pemasiri, M. Montazeri, R. Gass, L. M. Smith, H. E. Jackson, J. Yarrison-Rice, S. Paiman, Q. Gao, H. Hoe Tan, C. Jagadish, X. Zhang and J. Zou, *Nano Lett.*, 2009, **9**, 648–654.
- 59 J. Bao, D. C. Bell, F. Capasso, J. B. Wagner, T. Mårtensson, J. Trägårdh and L. Samuelson, *Nano Lett.*, 2008, **8**, 836–841.
- 60 P. Caroff, K. A. Dick, J. Johansson, M. E. Messing, K. Deppert and L. Samuelson, *Nat. Nanotechnol.*, 2009, **4**, 50–55.
- 61 R. E. Algra, M. A. Verheijen, M. T. Borgstrom, L.-F. Feiner, G. Immink, W. J. P. van Enckevort, E. Vlieg and E. P. A. M. Bakkers, *Nature*, 2008, **456**, 369.
- 62 J. Arbiol, A. Fontcuberta i Morral, S. Estradé, F. Peiró, B. Kalache, P. R. i Cabarrocas and J. R. Morante, *J. Appl. Phys.*, 2008, **104**, 064312.
- 63 A. De and C. E. Pryor, *Phys. Rev. B: Condens. Matter Mater. Phys.*, 2010, **81**, 155210.
- 64 I. Zardo, S. Conesa-Boj, F. Peiro, J. R. Morante, J. Arbiol, E. Uccelli, G. Abstreiter and A. Fontcuberta i Morral, *Phys. Rev. B: Condens. Matter Mater. Phys.*, 2009, **80**, 245324.
- 65 M. Heiss, S. Conesa-Boj, J. Ren, H.-H. Tseng, A. Gali, A. Rudolph, E. Uccelli, F. Peiró, J. R. Morante, D. Schuh, E. Reiger, E. Kaxiras, J. Arbiol and A. Fontcuberta i Morral, *Phys. Rev. B: Condens. Matter Mater. Phys.*, 2011, **83**, 045303.
- 66 B. Ketterer, M. Heiss, E. Uccelli, J. Arbiol and A. Fontcuberta i Morral, *ACS Nano*, 2011, **5**, 7585–7592.
- 67 J. Arbiol, S. Estradé, J. D. Prades, A. Cirera, F. Furtmayr, C. Stark, A. Laufer, M. Stutzmann, M. Eickhoff, M. H. Gass, A. L. Bleloch, F. Peiró and J. R. Morante, *Nanotechnology*, 2009, **20**, 145704.
- 68 G. Jacopin, L. Rigutti, L. Largeau, F. Fortuna, F. Furtmayr, F. H. Julien, M. Eickhoff and M. Tchernycheva, *J. Appl. Phys.*, 2011, **110**, 064313.
- 69 J. C. Johnson, H. Q. Yan, P. D. Yang and R. J. Saykally, *J. Phys. Chem. B*, 2003, **107**, 8816–8828.
- 70 M. A. Zimmler, D. Stichtenoth, C. Ronning, W. Yi, W. Narayanamurti, T. Voss and F. Capasso, *Nano Lett.*, 2008, **8**, 1695–1699.
- 71 M. T. Borgström, V. Zwiller, E. Mueller and A. Imamoglu, *Nano Lett.*, 2005, **5**, 1439–1443.
- 72 M. T. Björk, B. J. Ohlsson, T. Sass, A. I. Persson, C. Thelander, M. H. Magnusson, K. Deppert, L. R. Wallenberg and L. Samuelson, *Nano Lett.*, 2002, **2**, 87–89.
- 73 A. Pfund, I. Shorubalko, R. Leturcq and K. Ensslin, *Appl. Phys. Lett.*, 2006, **89**, 252106.
- 74 E. D. Minot, F. Kelkensberg, M. van Kouwen, J. A. van Dam, L. P. Kouwenhoven, V. Zwiller, M. T. Borgström, O. Wunnicke, M. A. Verheijen and E. P. A. M. Bakkers, *Nano Lett.*, 2007, **7**, 367–370.
- 75 T. Zang, N. A. Kotov and M. Giersig, *Science*, 2002, **297**, 237.
- 76 F. Wang, V. L. Wayman, R. A. Loomis and W. E. Buhro, *ACS Nano*, 2011, **5**, 5188.
- 77 H. Yu, L. Jingbo, R. A. Loomis, L. W. Wang and W. E. Buhro, *Nat. Mater.*, 2003, **2**, 517.

- 78 J. R. Heath and F. K. LeGoues, *Chem. Phys. Lett.*, 1993, **208**, 263.
- 79 J. D. Holmes, K. P. Johnston, R. C. Doty and B. A. Korgel, *Science*, 2000, **287**, 1471.
- 80 S. Koshihara, H. Noge, H. Akiyama, T. Inoshita, Y. Nakamura, A. Shimizu, Y. Nagamune, M. Tsuchiya, H. Kano and H. Sakaki, *Appl. Phys. Lett.*, 1994, **64**, 363.
- 81 H. Fujikura and H. Hasegawa, *J. Electron. Mater.*, 1996, **25**, 619.
- 82 H. Weman, P. Salmgren, K. F. Karlsson, A. Rudra, E. Kapon, D. L. Dheeraj, B. O. Fimland and J. C. Harmand, *J. Mater. Sci.: Mater. Electron.*, 2009, **20**, 94.
- 83 P. Kröger, M. Ruth, N. Weber and C. Meier, *Appl. Phys. Lett.*, 2012, **100**, 263114.
- 84 B. Gudden and R. Pohl, *Z. Phys.*, 1923, **17**, 331–346.
- 85 E. V. Kovarskii, *Fiz. Tverd. Tela*, 1977, **19**, 905–907.
- 86 V. K. Arora, *Phys. Rev. B: Condens. Matter Mater. Phys.*, 1981, **23**, 5611–5612.
- 87 P. M. Petroff, A. C. Gossard, R. A. Logan and W. Wiegmann, *Appl. Phys. Lett.*, 1982, **41**, 635–638.
- 88 L. T. Canham, *Appl. Phys. Lett.*, 1990, **57**, 1046–1048.
- 89 H.-J. Choi, J. C. Johnson, R. He, S.-K. Lee, F. Kim, P. Pauzaskie, J. Goldberger, R. J. Saykally and P. D. Yang, *J. Phys. Chem. B*, 2003, **107**, 8721–8725.
- 90 J. Arbiol, C. Magen, P. Becker, G. Jacopin, A. Chernikov, S. Schäfer, F. Furtmayr, M. Tchernycheva, L. Rigutti, J. Teubert, S. Chatterjee, J. R. Morante and M. Eickhoff, *Nanoscale*, 2012, **4**, 7517.
- 91 <http://departments.icmab.es/gaen/research/165>.
- 92 E. Uccelli, J. Arbiol, J. R. Morante and A. Fontcuberta i Morral, *ACS Nano*, 2010, **4**, 5985–5993.
- 93 X. Yan, X. Zhang, X. Ren, X. Lv, J. Li, Q. Wang, S. Cai and Y. Huang, *Nano Lett.*, 2012, **12**, 1851–1856.
- 94 M. Heiss, B. Ketterer, E. Uccelli, J. R. Morante, J. Arbiol and A. Fontcuberta i Morral, *Nanotechnology*, 2011, **22**, 195601.
- 95 B. A. Wacaser, K. Depperta, L. S. Karlsson and L. Samuelson, *J. Cryst. Growth*, 2006, **287**, 504–508.
- 96 C. Colombo, D. Spirkoska, M. Frimmer, G. Abstreiter and A. Fontcuberta i Morral, *Phys. Rev. B: Condens. Matter Mater. Phys.*, 2008, **77**, 155326.
- 97 D. Wasserman, S. A. Lyon, M. Hadjipanayi, A. Maciel and J. F. Ryan, *Appl. Phys. Lett.*, 2003, **83**, 5050–5052.
- 98 (a) E. Uccelli, M. Bichler, S. Nürnberger, G. Abstreiter and A. Fontcuberta i Morral, *Nanotechnology*, 2008, **19**, 045303; (b) E. Uccelli, S. Nürnberger, M. Bichler, G. Abstreiter and A. Fontcuberta i Morral, *Superlattices Microstruct.*, 2008, **44**, 425–430.
- 99 X. B. Niu, E. Uccelli, A. Fontcuberta i Morral and C. Ratsch, *Appl. Phys. Lett.*, 2009, **95**, 023119–023121.
- 100 Y.-W. Zhang, L. Lv and M. S. Bharathi, *Nano Lett.*, 2013, **13**, 538–542.
- 101 X. Yan, X. Zhang, X. Ren, H. Huang, J. Guo, X. Guo, M. Liu, Q. Wang, S. Cai and Y. Huang, *Nano Lett.*, 2011, **11**, 3941–3945.
- 102 X. Yan, X. Zhang, X. Ren, J. Li, X. Lv, Q. Wang and Y. Huang, *Appl. Phys. Lett.*, 2012, **101**, 023106.
- 103 M. Heiss, Y. Fontana, A. Gustafsson, G. Wüst, C. Magen, D. D. O'Regan, J. W. Luo, B. Ketterer, S. Conesa-Boj, A. V. Kuhlmann, J. Houel, E. Russo-Averchi, J. R. Morante, M. Cantoni, N. Marzari, J. Arbiol, A. Zunger, R. J. Warburton and A. Fontcuberta i Morral, *Nat. Mater.*, 2013, **12**, 439–444.
- 104 E. Russo-Averchi, M. Heiss, L. Michelet, P. Krogstrup, J. Nygård, C. Magen, J. R. Morante, E. Uccelli, J. Arbiol and A. Fontcuberta i Morral, *Nanoscale*, 2012, **4**, 1486–1490.
- 105 <http://departments.icmab.es/gaen/research/164>.
- 106 S. Bernal, F. J. Botana, J. J. Calvino, C. Lopez-Cartes, J. A. Perez-Omil and J. M. Rodriguez-Izquierdo, *Ultramicroscopy*, 1998, **72**, 135.
- 107 M. Ibáñez, R. Zamani, W. Li, A. Shavel, J. Arbiol, J. R. Morante and A. Cabot, *Cryst. Growth Des.*, 2012, **12**, 1085–1090.
- 108 See other 3D atomic models of complex nanostructures at: <http://www.icmab.cat/gaen/research/>.
- 109 J. Arbiol, A. Cirera, F. Peiro, A. Cornet, J. R. Morante, J. J. Delgado and J. J. Calvino, *Appl. Phys. Lett.*, 2002, **80**, 329.
- 110 M. I. B. Utama, M. de la Mata, C. Magen, J. Arbiol and Q. Xiong, *Adv. Funct. Mater.*, 2013, **23**, 1636–1646.
- 111 S. K. Lim, M. Brewster, F. Qian, Y. Li, C. M. Lieber and S. Gradečak, *Nano Lett.*, 2009, **9**, 3940–3944.
- 112 M. Brewster, X. Zhou, S. K. Lim and S. Gradečak, *J. Phys. Chem. Lett.*, 2011, **2**, 586–591.
- 113 M. Brewster, M. Y. Lu, S. K. Lim, X. Zhou, M. Smith and S. Gradečak, *J. Phys. Chem. Lett.*, 2011, **2**, 1940–1945.